JOURNAL OF MATERIALS SCIENCE **34** (1999) 2103–2111

The effect of fatigue damage on toughening of short-fiber-reinforced polymer composites

J. C. HA, A. T. YOKOBORI, JR.
Faculty of Engineering, Tohoku University, Aramaki Aoba, Aobaku, Sendai #980-8579, Japan

H. TAKEDA
Idemitsu Petrochemical Co., 1-1 Anezaki Kaigan, Ichihara, Chiba, #299-01, Japan

Fatigue fracture of fiber-reinforced polymer composites (FRP) occurs when microcracks are induced by debonding, pull-out and delamination at the interface between the matrix and fiber. This microcrack area increases with increase in fatigue cycles and a damage region is formed. In our previous paper, fatigue life of a short fiber-reinforced polymer composite consisting of glass fibers and polycarbonate matrix was found to be related not to the main crack growth behavior but to the progression behavior of the damage region. In this paper, using our proposed real time observational system, we performed detailed observations on the behavior of fatigue damage and clarified the mechanism of damage progression. Furthermore, mechanical considerations were performed by finite-element elastic-plastic stress analysis. The results mentioned above indicate that control of short fiber alignment makes it possible to release the stress concentration caused in the matrix, and disperse fatigue damage. This results in an enormous improvement in fracture toughness.

1. Introduction

In the case of fatigue fracture of fiber-reinforced polymer composites (FRP), microcracks are induced when debonding, pull-out and delamination occur at the interface between the matrix and fiber. This microcrack area increases with increase in fatigue cycles, and a damage region is formed [1–6]. As reported our previous paper, fatigue fracture life of a short fiber-reinforced polymer composite consisting of glass fibers and polycarbonate matrix is found to be related not to the main crack growth behavior but to the progression behavior of the damage region [5, 6]. Therefore, phenomenological clarification of the fatigue damage behavior of FRP is important to construct a physical model and a law of fatigue failure.

In this study, using the real-time observational experimental system proposed by us [5], we carried out detailed observations of the behavior of fatigue damage and clarified the mechanism of damage progression. Furthermore, mechanical considerations were performed by finite element elastic-plastic stress analysis.

2. Experimental procedure

2.1. Material specimen

The material used was a short fiber-reinforced polymer composite consisting of glass fibers (30 wt %) and a polycarbonate matrix. The diameter of each glass fiber was 13 μm, and the average length of each was 0.28 mm. The matrix was a general-purpose type bisphenol-A polycarbonate. The molecular weight (weight average M_w) was 27,800 and the polydispersity ratio was 2.78. The fiber was made of E glass and manufactured by winding melted glass through a bushing and then cutting it. Its surface was treated with a urethane-type coupling agent and aminosilane-type binder. The mechanical properties and composition of this material are shown in Table I. The mechanical properties of the matrix and fiber are shown in Table II. The materials were supplied as injection-molded plaques with dimensions of 70 mm by 70 mm by 2 mm. A thick molding has a preferred alignment of fibers in the flow direction of the surface layers, with fibers aligned transverse to the flow direction in the central layer [7]. However, the plaques supplied for these experiments were thin (2 mm). Therefore, in this case, the molding had a preferred alignment of fibers in the flow direction both on the surface and in the central layers. Furthermore, to avoid variations in the fiber alignment, each specimen was cut out from the central site of each plaque, as shown in Fig. 1. We used double-edged V-shaped notched specimens of 2 mm thickness with a 30° notch as shown in Fig. 2. To investigate the effect of anisotropy on the fatigue behavior of this material, we used three types of specimens that were cut from the plaques in the 0 (parallel), 45 and 90° (transverse) directions to the injection-molded flow direction. We refer to these as 0, 45, and 90° specimens.

2.2. Test method

Cyclic fatigue tests were carried out using a fatigue-testing machine that enables real-time observational experiments. This machine system was designed to

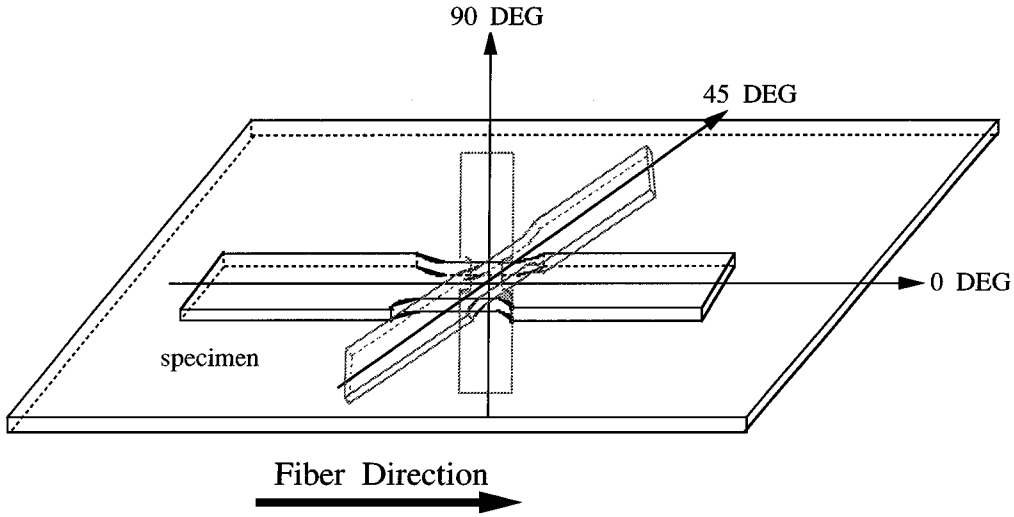

Figure 1 Cut out method of a specimen from the plaque (70 × 70 × 2 mm).

TABLE I Mechanical properties and composition of the composite material (polycarbonate matrix with glass fiber reinforcement)

Fiber content (wt %)	30
Specific gravity	1.42
Yield strength (MPa)	—
Tensile strength (MPa)	118
Modulus of elasticity (MPa)	5,880
Elongation at break (%)	3
Bending strength (MPa)	136

TABLE II Mechanical properties of the matrix and fiber

	Matrix	Fiber (glass)
Specific gravity	1.2	2.54
Yield strength (MPa)	62.0	2,940.0
Tensile strength (MPa)	71.0	3,430.0
Modulus of elasticity (MPa)	2,160.0	73,500.0
Elongation (%)	101.0	4.0

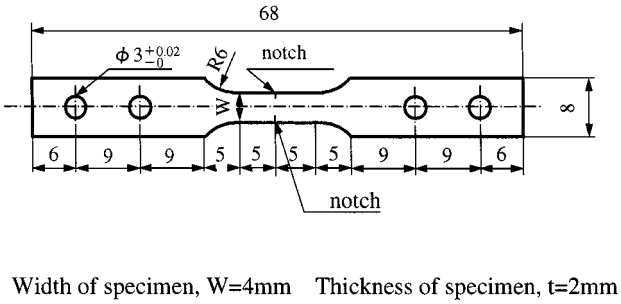

Width of specimen, W=4mm Thickness of specimen, t=2mm

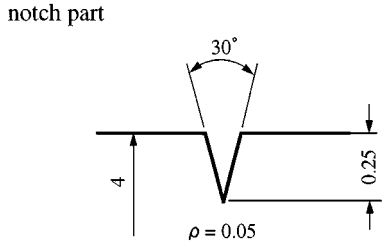

Figure 2 Double-edged V-shaped notched specimen.

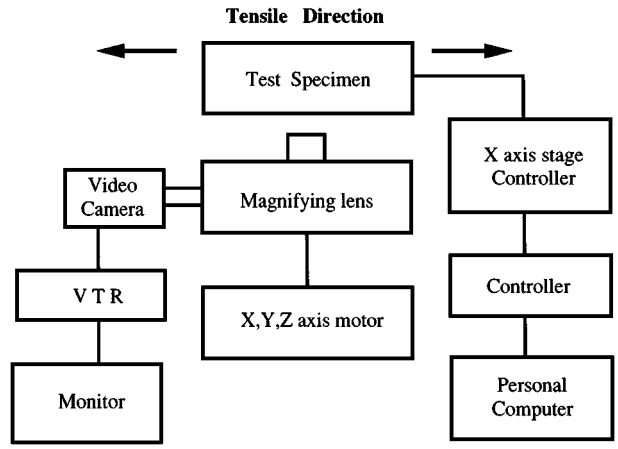

Figure 3 Schematic illustration of the observation system.

enable automatic observation of the mechanical behavior of deformation and damage accumulation around the crack tip during fatigue loading under computer control [5]. A schematic illustration of this system is shown in Fig. 3. Progression behavior of the fatigue damage was investigated by this real-time observational experimental technique, using a video microscope (Mitsubishi Electric Ltd.). Fatigue stress amplitude, $\Delta\sigma$, was set at $\Delta\sigma = 32$ MPa and the minimum gross stress, $\sigma_{\min}$ was zero, that is, the stress ratio $R(\sigma_{\min}/\sigma_{\max}) = 0$ for all tests. Tests were performed under atmospheric conditions, although the test temperature was maintained at $47 \pm 1\,^{\circ}$C to avoid any effects of room temperature variations on the mechanical behavior of the tests specimens.

3. Experimental results

3.1. Real-time observation of damage accumulation behavior

Progression behavior of the damage around the notch tip under fatigue testing was obtained by real-time observations using a video microscope. Photographs were obtained by transmitting rays through the specimen thickness from a source of light at the opposite side

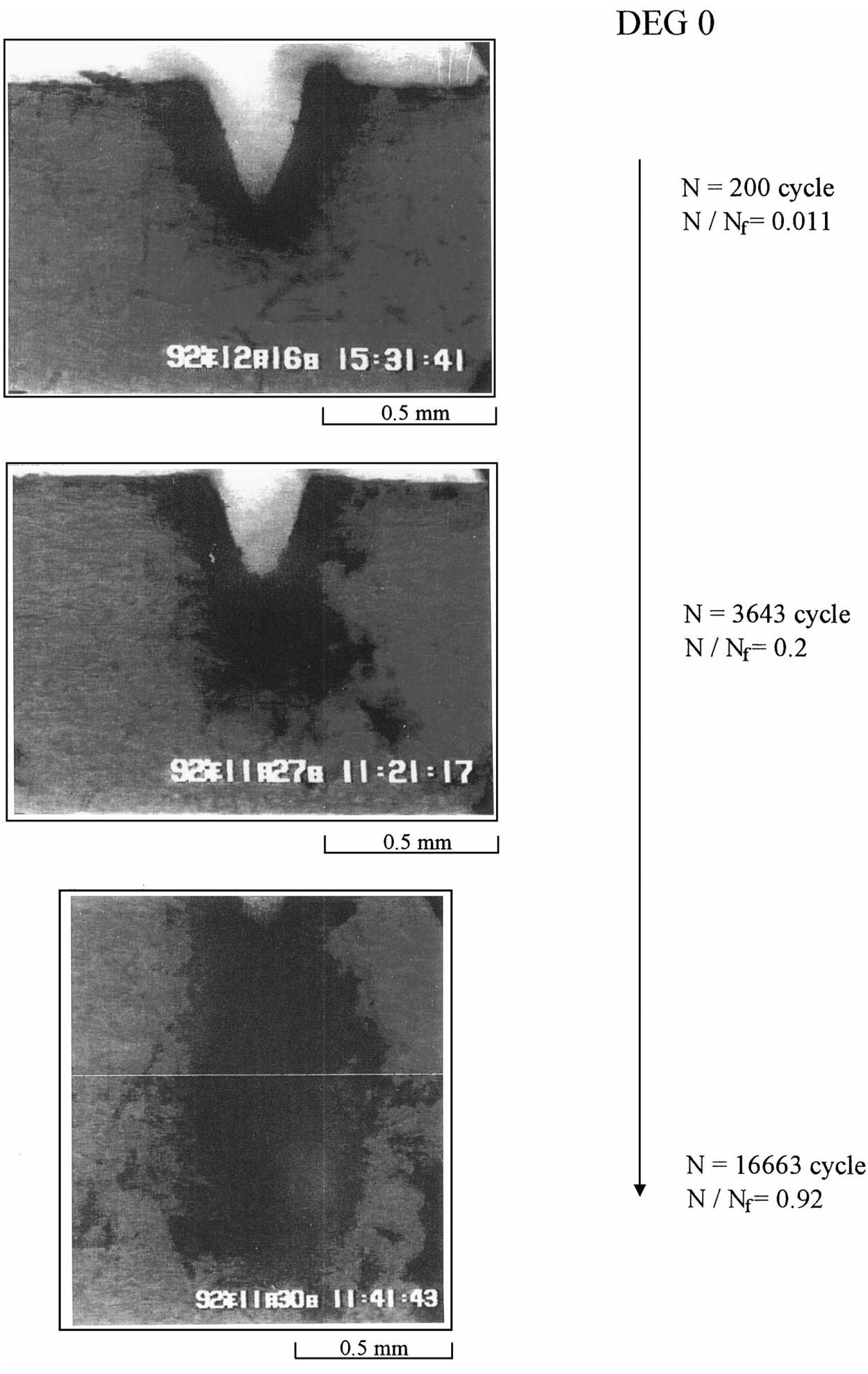

Figure 4 Real time observation on the progression behavior of damage around the notch tip (0° specimen).

of the specimen surface. Therefore the damage region is observed as a dark region, because of the scattering of light in this area due to microscopic fracture such as interfacial debonding and pull-out, fiber fracture, delamination and matrix cracking. The actual damage behavior is shown in Fig. 4. The damage region is divided into a main damage zone (deep dark zone) and a sub-damage zone (light dark region), which surrounds the main damage zone. Matrix cracking and local interfacial debonding mainly occur in the sub-damage zone. In the main damage zone, these phenomena were more advanced and sites of fiber fracture were discovered. Schematic diagrams of the progression behavior of the damage in the main and sub-damage zone are shown in Figs 5–7, respectively. Based on these in situ observations, the damage formation process is estimated.

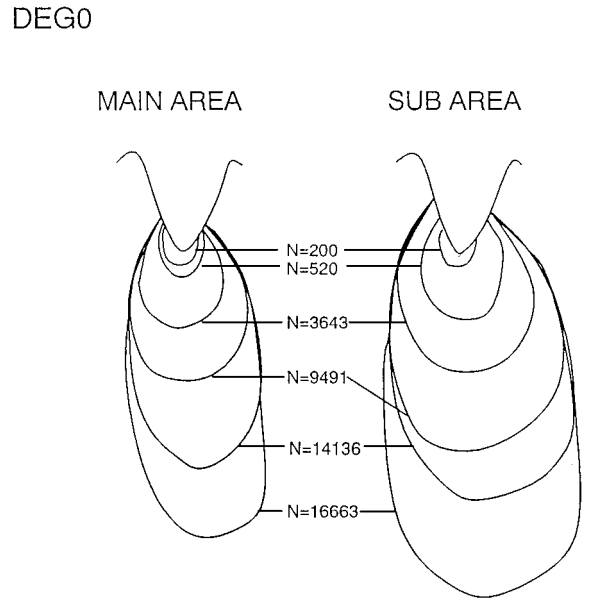

Figure 5 Schematic diagrams of the progression behavior of the damage in the main and sub-damage zone (0° specimen).

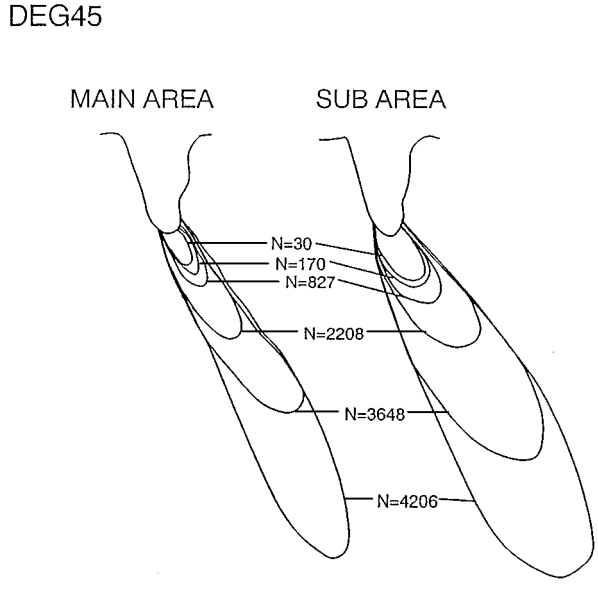

Figure 6 Schematic diagrams of the progression behavior of the damage in the main and sub-damage zone (45° specimen).

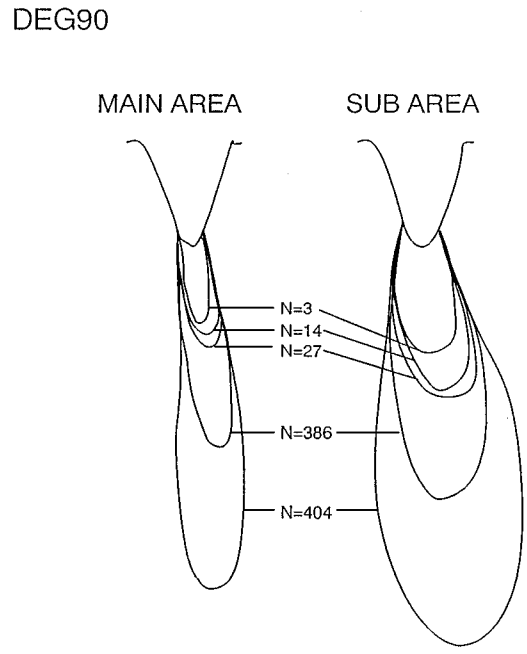

Figure 7 Schematic diagrams of the progression behavior of the damage in the main and sub-damage zone (90° specimen).

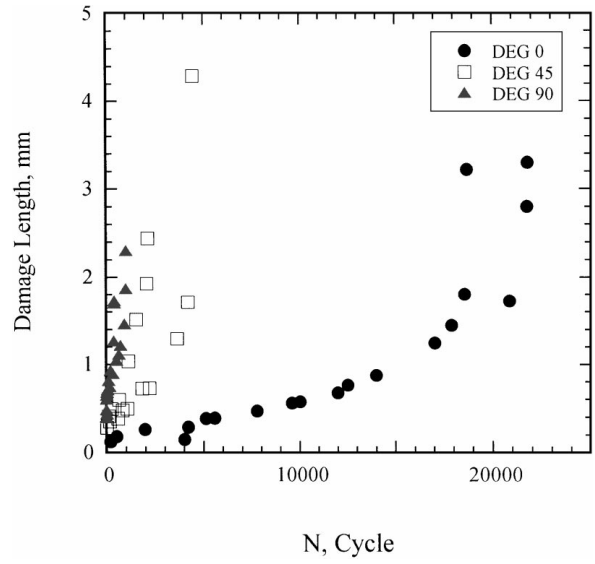

Figure 8 The relationships between the length of the damage zone and applied load cycles.

3.2. The length of the damage zone

The relationships between the length of the damage zone and applied load cycles are shown in Fig. 8. The length of the 90° specimen rapidly increases as compared with that of the 0° specimen. The final damage length of the 0° specimen is about 3.5 mm, which is equal to the initial ligament length of the specimen width. From this result, for the 0° specimen, the damage zone is found to spread through the specimen width before the occurrence of final fracture. In effect, it takes several load cycles before fracture finally occurs after the damage zone spread through the specimen width. This occurs as follows. The interfacial frictional stress between the fiber and matrix resists the pull-out of a fiber from the matrix, and thus controls the final rapid fracture of this material [8, 9]. The damage zone before final fracture for a 0° specimen is shown in Fig. 9. On

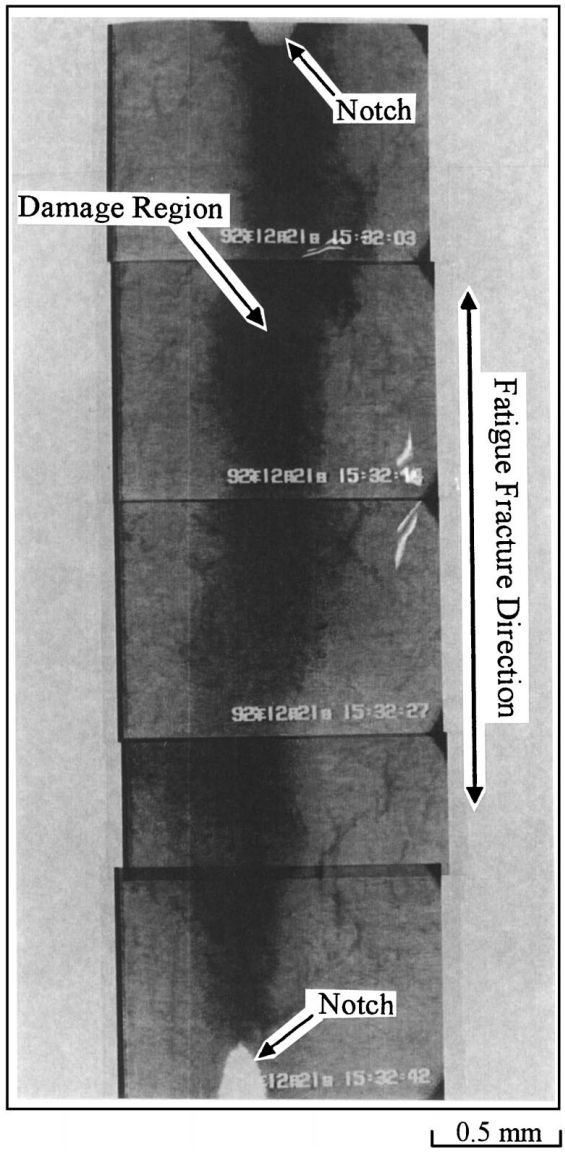

Figure 9 The behavior of damage before fracture (0° specimen).

the other hand, for a 90° specimen, final rapid fracture occurred before the spread of the damage region through the specimen width. The maximum damage length before final fracture is 0.7 times than that of a 0° specimen. The damage zone before final fracture for a 90° specimen is shown in Fig. 10. With respect to the 45° specimen, however, its fatigue fracture life is shorter than that of a 0° specimen, the maximum damage length is 1.3 times longer than that of a 0° specimen. This arises from the effect of the fiber alignment direction on damage formation, which results in the increase of the damage propagation distance due to inclination of its propagation direction.

3.3. Damage area

Accumulated damage areas up to fatigue fracture for the 0, 45, 90° specimens were plotted against fatigue cycle and normalized fatigue cycle, N and N/N_f as shown in Figs 11a and b, where N_f is the fatigue fracture life for each specimen. These results show that the damage area takes the minimum value for the 90° specimen and larger values for the 0° and 45° specimens. That is, the 90° specimen has the lowest toughness value. With regard to the 45° specimen, the fatigue fracture life, however, takes an intermediate value between those of the 0° and 90° specimens, its damage area takes the maximum value. This is caused by the inclined progress of the fatigue damage along the fiber direction. That is, each fatigue damage initiated from double-edged notch spreads over the whole ligament area of the specimen width without coalescing with one another. On the other hand, since the damage progression rate for a 45° specimen is much faster than that for a 0° specimen due to the coexistence of a delamination mechanism in the fiber [6], its fatigue fracture life becomes shorter as compared with that of the 0° specimen, which is controlled by the pull-out mechanism [5, 6]. The aspect

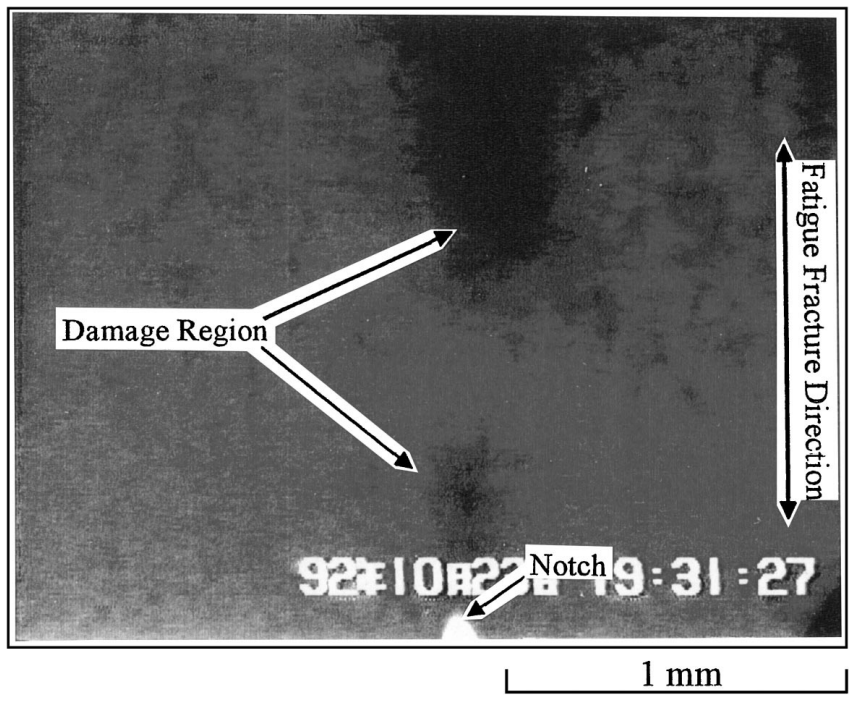

Figure 10 The behavior of damage before fracture (90° specimen).

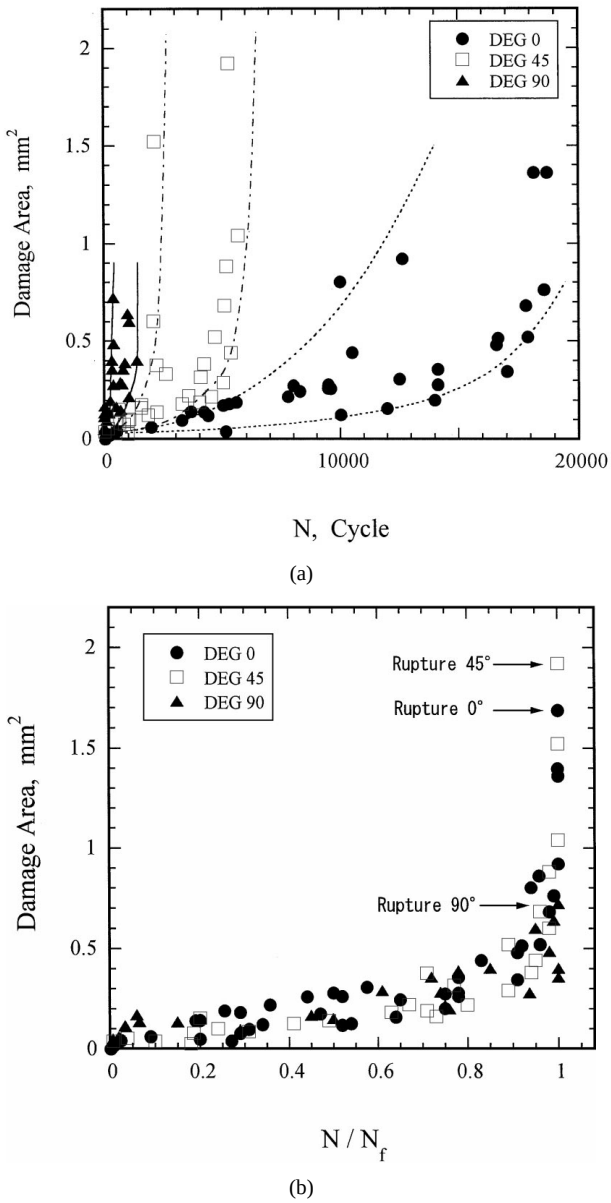

Figure 11 Accumulated damage area up to fatigue fracture for the 0, 45, 90° specimens plotted against (a) fatigue cycle, N, and (b) normalized fatigue cycle, N/N_f.

ratio of the fatigue damage area is plotted against normalized load cycles with respect to fatigue lifetime (N/N_f) as shown in Fig. 12. These results show that the 0° specimen takes the minimum aspect ratio of fatigue damage ($b/a = 1.5$) as compared with the 45° and 90° specimens. That is, fatigue damage of the 0° specimen spreads not only in the specimen width direction but also in the specimen axial direction and exhibits a two-dimensional shape pattern. On the other hand, the aspect ratios of the fatigue damage region for the 45° and 90° specimens are about 3.5. The damage regions exhibit a slender morphology extending in the fiber direction. From these results, fatigue damage for the 0° specimen is found to be dispersed preferentially in the direction of a specimen axis due to the short fiber reinforcement lying preferentially in the direction parallel to the specimen axis. On the other hand, for a 90° specimen, damage formation due to the interfacial delamination of the fibers aligned in the direction of specimen width becomes dominant and it progresses

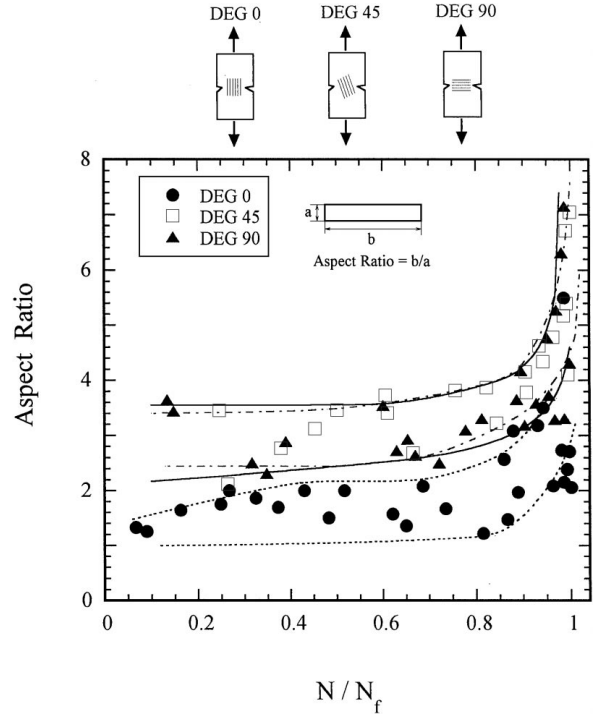

Figure 12 The aspect ratio of fatigue damage area plotted against normalized load cycles.

preferentially in the direction of specimen width [5, 6]. The damage formation mechanism of the 45° specimen is essentially the same as that of the 90° specimen [5, 6]. The progression characteristics of damage area for specimens with various fiber alignments were well characterized by a unique master curve as a function of notch opening displacement, D, as shown in Fig. 13 and it was written by Equation 1

$$\Delta\Phi/\Phi_0 = 0.13(D)^{0.7} \quad (1)$$

Φ_0 is the initial value of notch opening, i.e. the value before applying the load, and $\Delta\Phi = \Phi - \Phi_0$ is the increment of notch opening value Φ from the instant of load application.

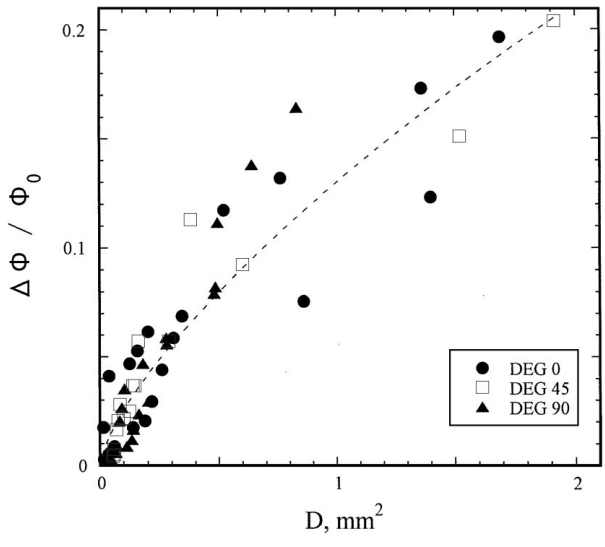

Figure 13 The relationship between fatigue damage and notch opening displacement.

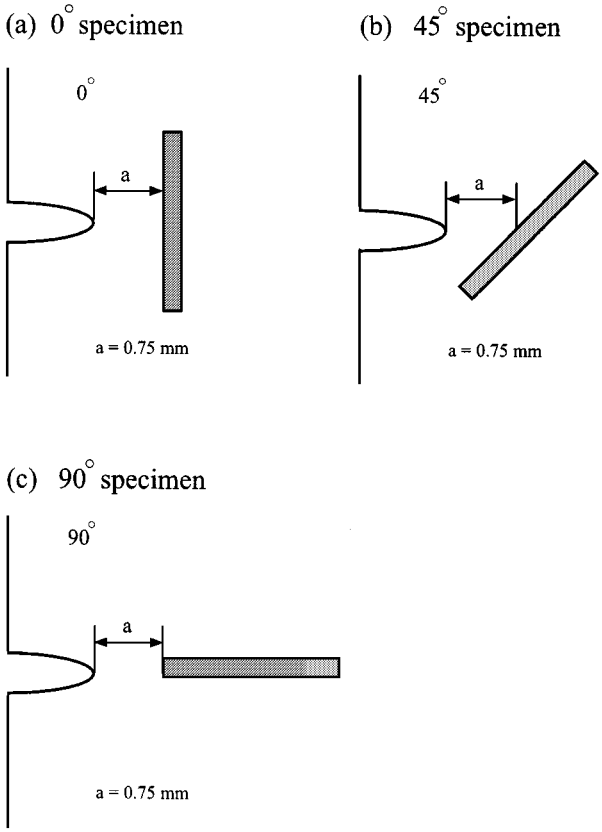

Figure 14 Mechanical models of the short-fiber alignment near the notch tip used for FEM analysis: (a) 0° specimen, (b) 45° specimen, and (c) 90° specimen.

4. Analytical results on the relationship between cumulative damage behavior and fiber alignment

Elastic-plastic stress analyses based on the finite-element method were performed to investigate the effect of reinforced fibers on stress concentration behavior around a notch tip. Analyses were performed for cases of 0, 45 and 90° alignment of short glass fibers. Simple mechanical models for short-fiber alignment near the notch tip were analyzed as shown in Fig. 14. The shape of the model was the same as that of the actual specimen. The distance between the notch tip and the center of glass fiber was 0.75 mm. The diameter and length of this representative glass fiber were 0.05 and 0.3 mm respectively. This diameter is four times larger than that of an actual fiber. Due to the symmetry of this mechanical model, we analyzed one-quarter of this model for 0° and 90° specimens and half for the 45° specimen. The number of elements and node points are shown in Table III and the mechanical properties used for FEM analysis are shown in Table IV.

By using FEM software on the elastic-plastic stress analyses by Yamada (EPIC) [10], we modified this software so that we can perform cyclic loading elastic plastic analysis [11]. Local damage is considered to be formed in the high-equivalent stress region [12–15]. Mechanical analysis in the damage region was performed under the condition of perfect plastic properties, since, in this region, low-resistance inelastic deformation is considered to occur, due to pull out and

TABLE III The number of elements and node points used for FEM analysis

	No. of elements	No. of nodes
0°	888	482
45°	1,840	975
90°	903	490

TABLE IV Mechanical properties used for FEM analysis

	Young's modulus (MPa)	Poisson's ratio	Yield strength (MPa)
Polycarbonate	2,160	0.3	62
Glass	73,500	0.22	2,940

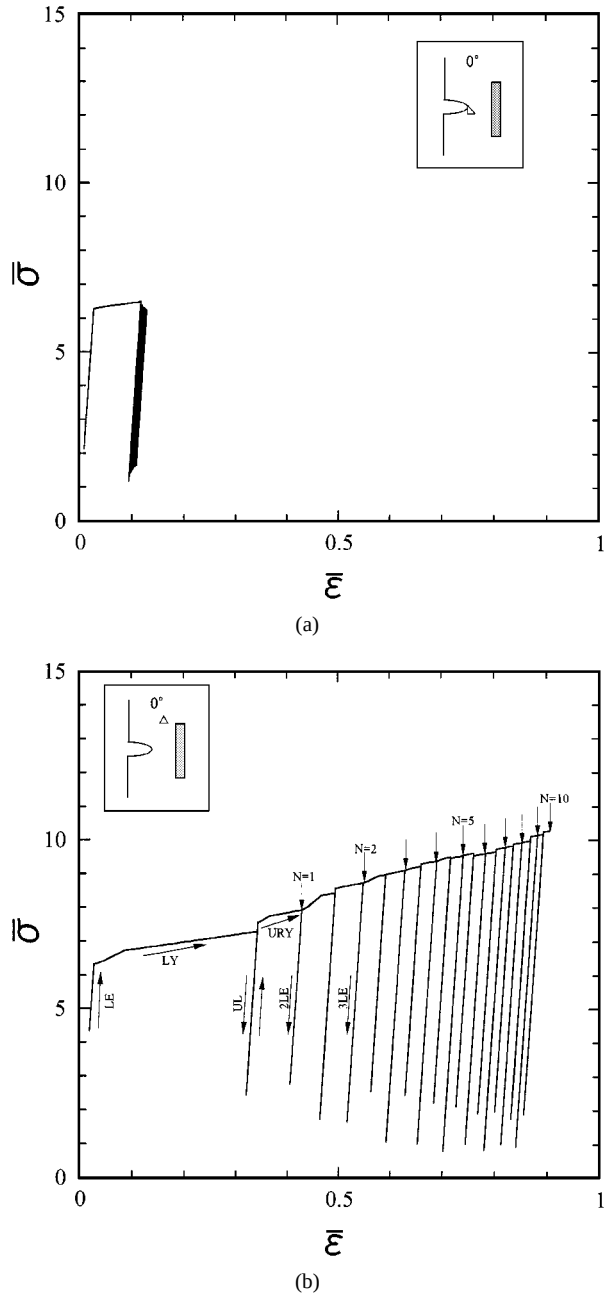

Figure 15 (a) Cumulative behaviors of plastic strain energy due to equivalent stress and strain under a cyclic loading and unloading process, and (b) LE is loading process under elastic condition, LY is loading process under plastic condition, UL is unloading process and URY is reyielding during unloading. $N = 1$ means the completion of the 1st load cycle.

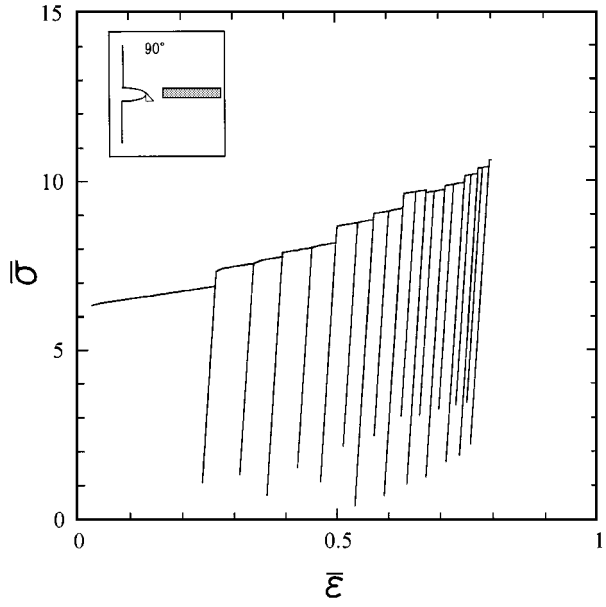

Figure 16 Cumulative behaviors of plastic strain energy due to equivalent stress and strain under a cyclic loading and unloading process.

delamination at the interface between a fiber and matrix [16–19]. Therefore, analyses of entire structure were performed by using an elastic perfect plastic constitutive law [20]. Cumulative behaviors of plastic strain energy due to equivalent stress and strain under a cyclic loading and unloading process are shown in Figs 15 and 16. Each characteristic of strain energy accumulation is shown with a mark in each figure. These analyses provide the following results. For the 0° specimen, the value of W_p does not increase at the tips of a notch or a fiber end, but increases in an intermediate region between them (Fig. 15a, b). On the other hand, for the 90° and 45° specimens, the value of W_p increases at the tip of a notch. This behavior is much more prominent in a 90° specimen. Local damage, as is reported in this paper, occurs in the region of increasing W_p. From these results, for the 0° specimen, stress concentration around a notch tip is found to be released due to the existence of short fibers and local damage is dispersed around the notch tip. On the other hand, for the 90° specimen, stress concentration occurs around the notch tip due to the mechanical interaction between the tips of the fibers and the notch. Consequently, delamination occurs at the interface between fiber and matrix, which results in the progression of damage formation perpendicular to the tensile stress. From the results mentioned above, for a 0° specimen, fiber structure induces dispersion of damage which is composed of local fracture, that is, multiple crack initiation [16–19]. This causes the shielding effect on main crack growth, that is, the release of stress concentration at the notch tip, and prolongation of fatigue fracture life. The concept of multiple crack initiation is shown to be important for improving the fracture toughness of concrete [21]. This should be a common concept for general engineering materials. Therefore, dispersion of local fracture (damage) by multiple crack initiation [21] occurring in the 0° specimen has a significant mechanism for the improvement of fracture toughness.

5. Conclusions

In situ observations of fatigue damage progression in a notched specimen of short-fiber-reinforced polymer composites was performed and the following conclusions were obtained.

1. The length, area and aspect ratio of damage strongly depend on the direction of the fiber alignment and the applied load.

2. Stress concentration at the notch tip is released by the alignment of short fibers on parallel to the direction of load application and damage is dispersed. Furthermore, after fatigue damage spreads through the specimen width, final fracture does not occur at once and it requires several load cycles before final fracture occurs. This is caused by the interfacial frictional force between the fiber and matrix, which constrains final rapid fracture due to pull-out. This structure improves fracture toughness as a composite material.

3. Stress concentration at the notch tip is intensified by the neighboring fibers when the fibers are aligned in a direction perpendicular to that of load application. It promotes final rapid fracture due to delamination, and final fracture occurs before fatigue damage spreads through the specimen width.

4. From the results mentioned above, control of the short fiber alignment makes it possible to release stress concentration caused in the matrix and disperse fatigue damage due to multiple crack initiation. The use of this technique for multiple crack initiation, for dispersion of fracture damage, results in an enormous improvement in fracture toughness.

Acknowledgements

We appreciate the financial aids for the Japan Society for Promotion of Science of the RFTF program, 97R12101 and Professor Takeo Yokobori (Teikyo University) for useful discussion. Thanks also should be made to Idemitsu Petrochemical Co. for supply of the material used.

References

1. R. D. JAMISON, K. SHULTE, K. L. REIFSNIDER and W. W. STINCHCOMB, Effect of Defects in Composite Materials, ASTM STP 836 (1984) 21–55.
2. T. AOKI, T. KUBO, K. KONDO and S. KOBAYASHI, *J. Japanese Soc. Comp. Mater.* **15**(3) (1989) 122–131.
3. A. POURSATIP and P. W. R. BEAUMONT, in "Mechanics of Composite Materials," edited by Z. Hasin and C. T. Herahovich (Pergamon Press, 1983) pp. 449–456.
4. H. C. KIM and L. J. EBERT, *J. Composite Mater.* **12** (1978) 139–152.
5. A. T. YOKOBORI, Jr., H. TAKEDA, T. ADACHI, J. C. HA and T. YOKOBORI, in "Fiber, Matrix and Interface Properties, ASTM STP 1290," edited by C. J. Spragg and L. T. Drzal (1996) 152–167.
6. A. T. YOKOBORI, Jr., J. C. HA, T. TANI and H. TAKEDA, *J. Japanese Soc. for Strength and Fracture of Mater.* **29**(4) (1995) 113–120.
7. R. W. LANG, J. A. MASON and R. W. HERTZBERG, *J. Mater. Sci.* **22** (1987) 4015–4030.
8. L. J. BROUTMAN, in Proc. of the 25th SPI/RP Annual Technology Conference Paper 13-D (Society of the Plastics Industry, New York, 1970).

9. D. HULL, "An Introduction to Composite Materials" (Cambridge Univ. Press, 1982); translation by H. Miyairi, K. Ikegami and I. Kinbara (Boifukan, 1984).
10. Y. YAMADA, "Plasticity and Viscoelasticity" (Baifukan Publishers, 1972) (in Japanese).
11. A. T. YOKOBORI, Jr. and T. ISOGAI, Trans. of the Annual Meet of Japanese Soc. for Mechanical Engineers, Vol. A, No. 910–917 (1991) pp. 72–74.
12. L. M. KACHANOV, "Introduction to Continuum Damage Mechanics" (Martinus Nighoft Publishers, The Netherlands, 1986).
13. J. HULTS, in "Materials and Engineering Design the Next Decade," edited by B. F. Dyson and D. R. Hayhurst (The Institute of Metals, London, 1989) p. 29.
14. J. L. BASSANI and D. F. HAWK, in "International Seminar on High Temperature Fracture Mechanisms and Mechanics," edited by M. B. Mecamat, and F. D. Danbrine (Dourdan, France, 1987) pp. 19–40.
15. A. LEVY and J. M PAPAZIAN, *Acta Metall. Mater.* **39**(70) (1991) 2255–2266.
16. K. FRIEDRICH, "Fracture Mechanical Behaviour of Short Fibre Reinforced Thermoplastics," Furtshr-Blr VDI-Zeitshr, Series, No. 18 (VDI-Verlag, Dusseldorf, 1984).
17. C. LHYMN, *J. Mater. Sci. Lett.* **4** (1985) 1323.
18. K. TAKAHASHI and N. S. CHOI, *J. Mater. Sci.* **26** (1991) 4648.
19. N. S. CHOI and K. TAKAHASHI, *ibid.* **31** (1996) 731.
20. M. ZAKO, "Numerical Mechanics of Composite Materials" (Yokendo, 1989).
21. H. MIHASHI and N. NOMURA, *Cement & Concrete Composites* **14** (1992) p. 91.

Received 6 August
and accepted 13 October 1998